Transient electric birefringence in suspensions of single-walled carbon nanotubes

K. J. Donovan* and K. Scott
Physics Department, Queen Mary, University of London, Mile End Road, London E1 4NS, United Kingdom
(Received 1 August 2005; published 30 November 2005)

In the torque created by an electric field, highly polarizable single-walled carbon nanotubes, suspended in dichloroethane, rotate and align with the field creating a transient induced birefringence (TEB). The magnitude of the birefringence, Δn, is followed in time by the switching of a square voltage pulse across the suspension and following the time evolution of the transmitted light through crossed polarizers. The variation of the magnitude of Δn with applied electric field and nanotube concentration is reported. We find that in spite of the polydisperse nature of the nanotube suspensions a single exponential growth is sufficient to describe the evolution of the birefringence, as the field is switched on. The low field reciprocal rise time of Δn varies as the square of the applied electric field, and the low field magnitude is proportional to the square of the applied electric field at low fields. These observations are discussed in the light of the classic Kerr effect. The TEB is shown to be dominated by induced dipole moments on the metallic nanotubes that form part of the suspension.

DOI: 10.1103/PhysRevB.72.195432 PACS number(s): 81.07.De, 83.10.Mj, 83.10.Ff, 82.70.Kj

I. INTRODUCTION

Single-walled carbon nanotubes (SWNTs) have generated much interest since their identification in 1991 by Iijima.[1] This is largely because this allotrope of carbon has remarkable properties regarding its strength and electronic transport. Many of these properties were first posited as theoretical possibilities before later being confirmed experimentally.

The SWNTs, both semiconducting and metallic, have a very large polarizability which is expected to be several orders of magnitude larger for the metallic tubes.[2] This differential polarizability has been shown to be useful as a potential route into separation of metallic from semiconducting SWNTs using the technique of dielectrophoresis.[3,4]

The high polarizability is also seen to have consequences in electronic transport measurements on SWNTs in suspension,[5,6] where applied electric fields necessary for the transport measurements tend to align the nanotubes with the field affecting the magnitude of transient photocurrent signals measured on the SWNTs.[6] Also the metallic tubes aligning in the electric field tend to form filaments that eventually extend across the measuring cell and cause short circuits to occur.[5] For a better understanding of the electronic transport results, an understanding of the timescale upon which alignment occurs is necessary and how these times may be controlled experimentally.

The alignment is, of course, useful in its own right as electric fields are increasingly being suggested and demonstrated as solutions to the problem of placement of single nanotubes in desired locations,[7–9] an important achievement necessary for progress to be made in the use of SWNTs in nanoelectronics, a widely held ambition.[10]

In order to study this field alignment further we will use the effect of field-induced transient birefringence to observe the alignment in real time, a technique that has been little used so far in the study of SWNTs. Indeed we are aware of only one other work on the Kerr effect on SWNTs that has been published to date.[11] In that work an ac field was used on much more concentrated SWNT suspensions. No Kerr coef-

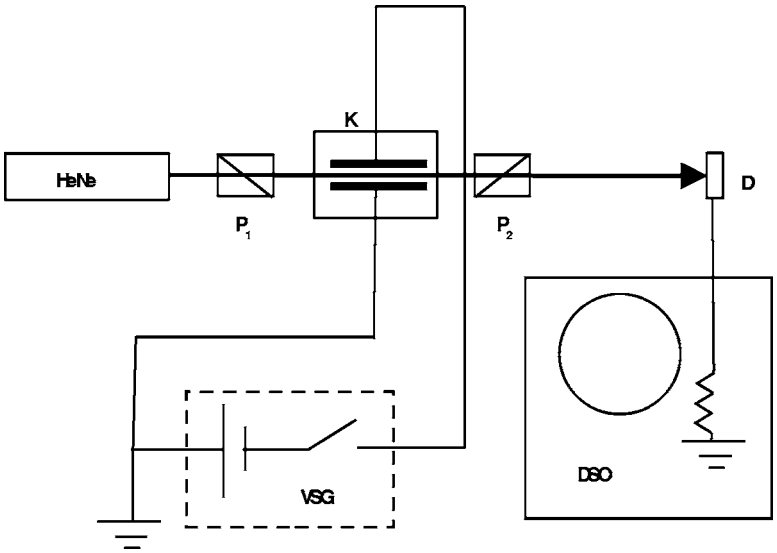

FIG. 1. The Kerr cell **K** contains the nanotube suspension between two electrodes in the cell applying a uniform E field from a voltage step generator, VSG. The cell is between two crossed polarizers, $\mathbf{P}_1$ and $\mathbf{P}_2$. Light from a helium neon laser passes through both polarizers and cell. The transmitted light is attenuated by neutral density filters, NDF, before being measured by a pin diode detector, **D**. The output of the diode is displayed on a digitizing oscilloscope, DSO.

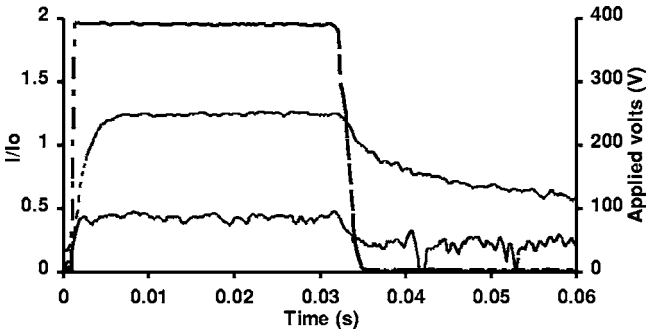

FIG. 2. The voltage step is shown along with the change in transmission due to the presence of dichloroethane alone in the Kerr cell. Also shown for comparison is an example of a small SWNT signal with wt fraction 0.57×10^{-6} and $E=1.6\times10^{5}$ V m^{-1}.

ficient was found, and the dynamics of the effect was not studied.

II. EXPERIMENT

The SWNTs used in these experiments, obtained commercially from Carbolex, were synthesized by the arc discharge method and have a diameter of 1.4 nm±0.2 nm. Their length is ill defined but the longest are on the order of microns in length. They were suspended in dichloroethane, after dispersal with an ultrasonic probe, a suspending medium known to disperse the nanotube material well and to break up SWNT ropes into single nanotubes capable of being imaged using STM techniques.[12] Very low concentrations were used to limit tube-tube interaction, and the suspension was contained in a glass cuvette of 1 cm path length. The experimental setup for measuring birefringence is shown in Fig. 1. A pair of parallel plate electrodes separated by $D=2.5$ mm were held in the suspension in the cuvette and provided a uniform electric field. The electrodes had a height of 4 mm and were able to provide an applied electric field along a path of length $l=9$ mm within the cuvette.

One of the electrodes was connected to a voltage pulse generator and the electric field was applied as a square voltage pulse of variable amplitude, from 50 V up to 2 kV, for a controllable duration, typically 30 milliseconds, depending on the experimental requirements. The other electrode was grounded. A highly stable 5 mW HeNe laser beam was plane polarized at 45° to the electric field direction using a Glan-Thompson polarizer between the cell and laser, and a second polarizer set at 90° to the first was placed after the cell followed by a Si photodiode detector. The output from the photodiode was monitored with a digitizing sampling oscilloscope (DSO). Neutral density filters were used as and when necessary in order to prevent saturation of the detector and maintain it in its linear response regime. With this setup we were able to measure birefringence of less than 10^{-8}. One of the main limits on our sensitivity was the competing birefringence of dichloroethane at low nanotube concentration. At low fields the accuracy of alignment of the two polarizers gives rise to a systematic error in the birefringence measurement. Figure 2 shows the voltage step and the background transient electric birefringence, TEB, from the dichloroethane and a SWNT suspension at lowest voltage and concentration for comparison.

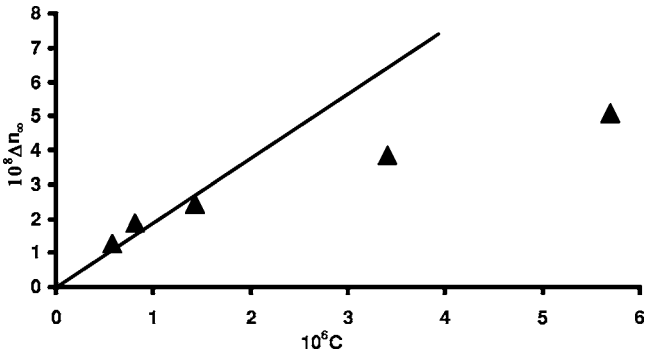

FIG. 4. Long time birefringence Δn_∞ vs concentration from the data of Fig. 3. The line fits the data at low concentration.

Because of the large polarizabilities possessed by SWNTs there was a dipole moment induced by the applied electric field followed by a partial alignment of the dipole with that field as the SWNTs are free to re-orientate in suspension. With alignment the previously homogenous suspension becomes birefringent with the refractive index, $n_\parallel$, parallel to the electric field direction being somewhat larger than the refractive index $n_\perp$ perpendicular to the field direction. The

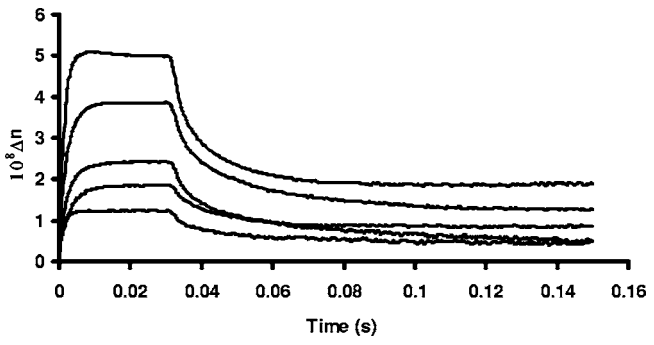

FIG. 3. Transient electric-field-induced birefringence signals at varying concentrations, from top to bottom, 5.7, 3.4, 1.43, 0.81, and 0.57×10^{-6} weight fraction of nanotubes in DCE. The electric field is 1.6×10^{5} V m^{-1}.

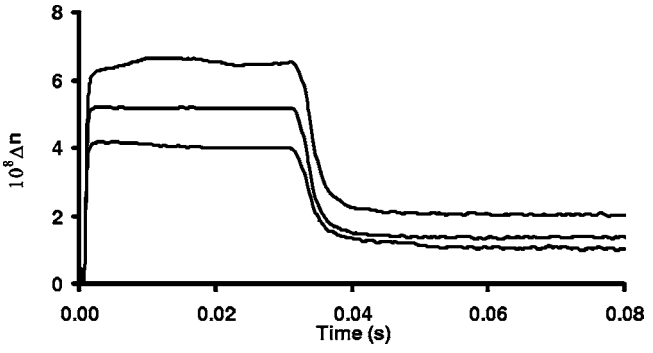

FIG. 5. Transient electric-field-induced birefringence signals at varying concentrations, from top to bottom, 5.7, 3.4, 0.81×10^{-6} weight fraction of nanotubes in DCE. The electric field is 8.0×10^{5} V m^{-1}.

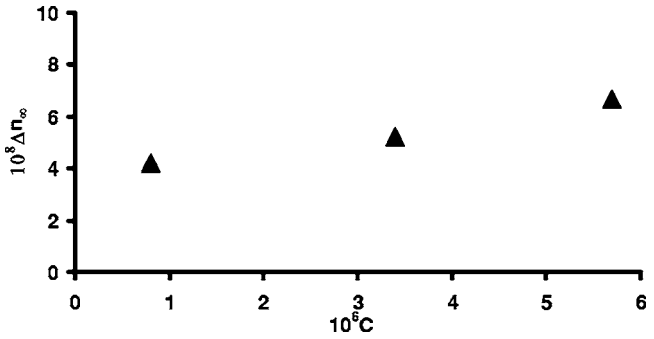

FIG. 6. Long time birefringence Δn_∞, vs concentration at 8.0×10^5 V m^{-1} taken from the data of Fig. 5.

light emerging from the cell was thus elliptically polarized and the transmission of the polarizer pair increased. Measurement of the transmission, T, enabled us to find the TEB of the suspension, $\Delta n = (n_\parallel - n_\perp)$

$$T = \frac{I_{Out}}{I_{In}} = \sin^2(\boldsymbol{\Delta\varphi} + \boldsymbol{\delta}) = \sin^2(\boldsymbol{\Delta} n k_0 l + \boldsymbol{\delta}), \tag{1a}$$

$$\Delta n = \frac{\arcsin(\sqrt{T}) - \boldsymbol{\delta}}{k_0 l} = \frac{\arcsin(\sqrt{T})}{k_0 l} - \frac{\boldsymbol{\delta}}{k_0 l}, \tag{1b}$$

where I_{Out} is the output measured after the second polarizer and I_{In} is the input measured at the far side of the cell with the second polarizer removed and no voltage is applied. $\Delta\varphi$ is the phase difference between the two components of polarization parallel and perpendicular to the applied electric field after traversing the cell. k_0 is the wave vector of the HeNe laser light in free space. $\boldsymbol{\delta}$ is a measure of the misalignment of the two polarizers.

Assuming $\boldsymbol{\delta}=0$ we are able to measure the variation of Δn with an applied electric field and to change the concentration of nanotubes and find how this changes the value of Δn at a given field. Furthermore we can find the dynamic response of the SWNTs to the application of a driving torque and also to observe the motion of the tubes driven by Brownian forces, unconstrained by any externally applied force, as they once again randomize their orientation after the field is turned off.

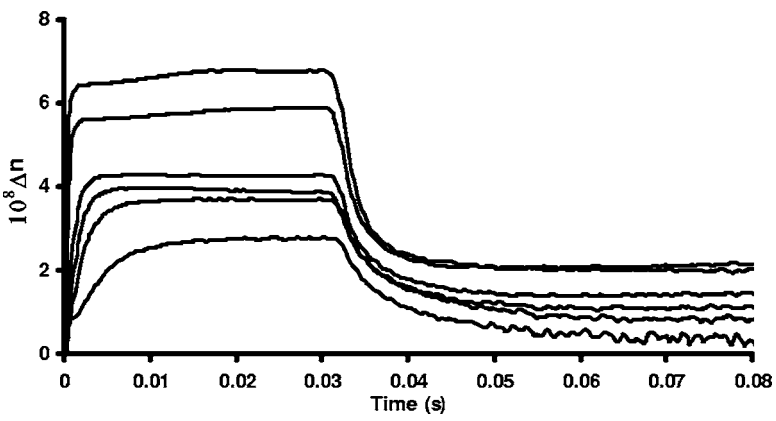

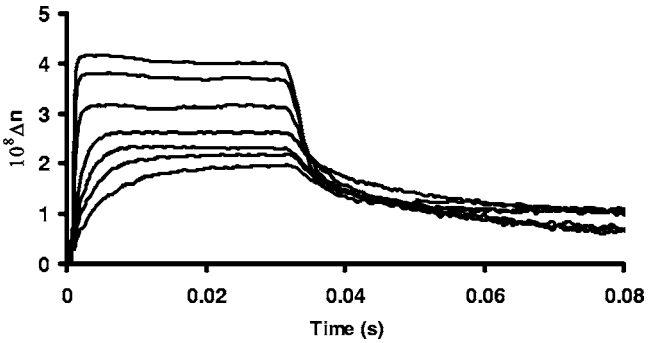

FIG. 7. Transient electric-field-induced birefringence signals at varying electric fields, from top to bottom, 8.0, 6.4, 4.0, 2.0, 1.6, 1.2, and 0.8×10^5 V m^{-1} at 0.81×10^{-6} weight fraction of nanotubes in DCE.

III. RESULTS

Using Eq. (1) and assuming $\boldsymbol{\delta}=0$ the measurement of T has been converted to Δn in the results presented, giving a direct measure of the birefringence.

A. Concentration dependence

Figure 3 shows the time response of the birefringence, $\Delta n(t)$, to an electric field, $E = 1.6 \times 10^5$ V m^{-1}, applied in the form of a rectangular voltage pulse, at several SWNT concentrations from 0.57×10^{-6} to 5.7×10^{-6} by weight fraction in dichloroethane, and Fig. 4 shows the steady state birefringence, Δn_∞, from Fig. 3 plotted vs concentration C. Equivalent results are shown in Figs. 5 and 6 at the five times higher field of $E = 8.0 \times 10^5$ V m^{-1}.

We need to begin by establishing which concentration regime we are in. A nanotube of length $L = 1$ μm and 1.4 nm diameter has a molecular weight of 1.95×10^6 and a mass of 3.23×10^{-21} kg, the density of dichloroethane is 1.26 g/cm^3, therefore, given a nanotube weight fraction of 1×10^{-6} there will be a number density $n = 3.9 \times 10^{11}$ cm^{-3}. The length per tube $\mathcal{L}$ is then given by $1/\sqrt[3]{N} = 1.4 \times 10^{-4}$ cm $= 1.4$ μm. We have assumed tubes of length 1 μm and therefore at that concentration, in the middle of the range we have used, we are on the boundary of dilute and/or semidilute solution. We are thus close to the regime where weak tube-tube interaction may play a role in the experiments.

FIG. 8. Transient electric-field-induced birefringence signals at varying electric fields, from top to bottom, 6.4, 4.0, 2.0, 1.6, 1.2, and 0.8×10^5 V m^{-1} at 5.7×10^{-6} weight fraction of nanotubes in DCE.

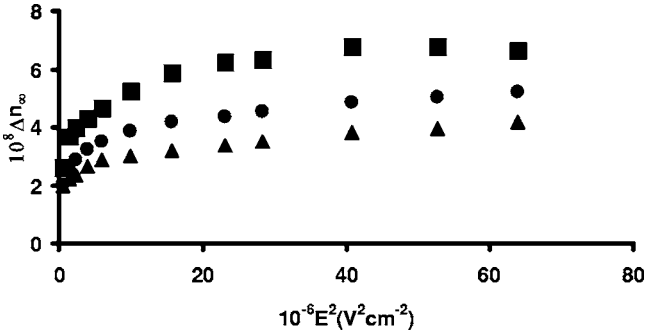

FIG. 9. The long time birefringence Δn_∞ is shown as a function of the square of the electric field at 0.8×10^{-6} weight fraction ▲, 3.4×10^{-6} weight fraction ●, and 5.7×10^{-6} weight fraction ■.

The birefringence appears approximately linear in concentration at lower fields and low concentrations, Fig. 4, whereas at higher fields, Fig. 6, the birefringence is tending to saturate as concentration is increased.

B. Electric field dependence

Figure 7 shows the time response $\Delta n(t)$ at low concentration of 0.81×10^{-6} wt fraction, at several fields while Fig. 8 shows the time response $\Delta n(t)$ at higher concentration of 5.7×10^{-6} wt fraction at several fields. As the concentration is increased, at higher fields the value of Δn does not find a steady value but after a rapid rise shows some sign of instability as seen in Fig. 8. As we noted previously, on going from 0.81 to 5.7×10^{-6} wt fraction we are crossing the dilute and/or semidilute boundary and the changes noted between the results of Figs. 7 and 8 may reflect this change. In Fig. 9 Δn_∞ is shown at low, intermediate, and high concentrations as a function of the square of the electric field. The birefringence tends rapidly to the saturation at the fields used in these experiments. This saturation with the field is also reflected in the nonlinearity of the birefringence with concentration at high fields remarked upon earlier with regard to Fig. 6. To observe Kerr behavior it is necessary to go to lower fields and Fig. 10 shows $\Delta n(t)$ at low fields for a suspension of wt fraction 1.17×10^{-6}. The dependence of

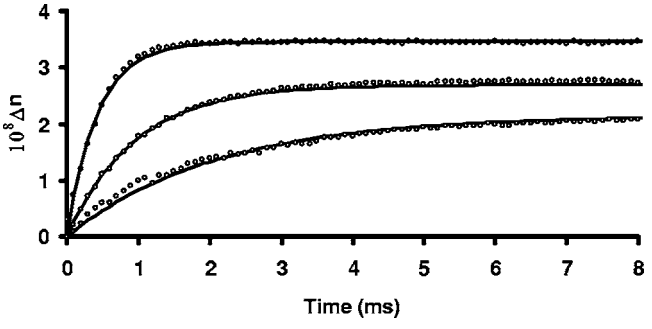

FIG. 10. The growth in transient electric-field-induced birefringence signals at varying electric fields, from top to bottom, 3.2, 1.6, and 1.0×10^5 V m^{-1} at 1.17×10^{-6} weight fraction of nanotubes in DCE. The open circles are the data and the bold lines are fits to Eq. (2).

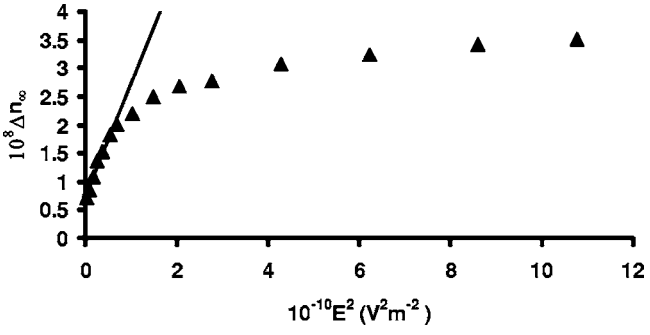

FIG. 11. The long time birefringence Δn_∞ plotted against the square of the electric field going to low electric fields at a weight fraction of 1.17×10^{-6} from data similar to that of Fig. 10.

Δn_∞, the steady state birefringence attained when the electric field has been on for long times, on E^2 found from data similar to that of Fig. 10 is shown in Fig. 11 going to very low fields. We have fitted the rise after switching on the voltage to

$$\Delta n(t) = \Delta n_\infty\left(1 - \exp\left(-\frac{t}{\tau_R}\right)\right), \tag{2}$$

and find values for τ_R and Δn_∞ from such fits.

At low fields the magnitude of the birefringence is found to be proportional to the square of the field with an intercept on the birefringence axis. The intercept corresponds to a very small polarizer misalignment that is unavoidable. In Fig. 12 the value of Δn_∞ is plotted against E^{-2} and a value of $\Delta n_\infty = 3.8\times10^{-8}$ is found from extrapolation to infinite field or full alignment.

C. Rate of field induced orientation

Figure 13 shows the exponential growth rate τ_R^{-1} found from fitting data such as that in Fig. 10, plotted against the square of the electric field. At low electric fields the alignment rate is found to be proportional to E^2.

D. Rate of randomization

The decay of the birefringence seen in Figs. 3, 5, 7, and 8 immediately after the electric field is turned off is complex and depends among other things on the state of the suspen-

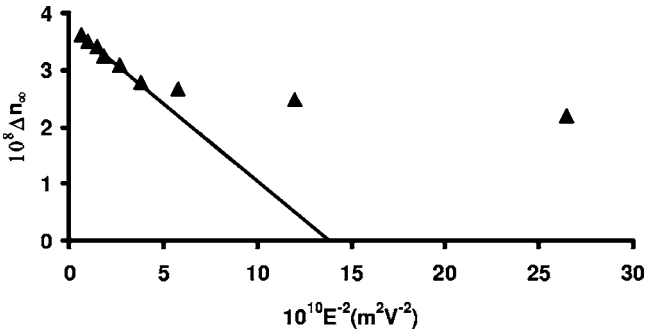

FIG. 12. Δn_∞ plotted against the reciprocal of the square of the electric field with the data taken from Fig. 11.

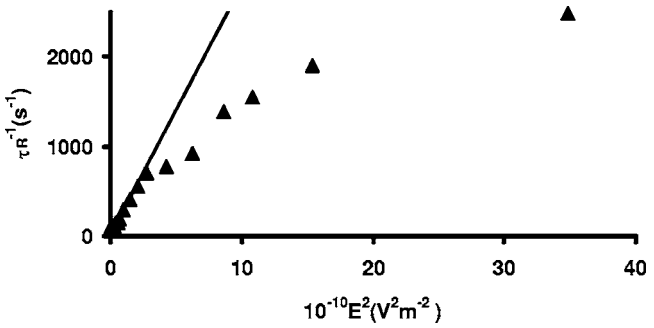

FIG. 13. The reciprocal risetime, $\tau_{R^{-1}}$, found from the data similar to that of Fig. 10 fitted to Eq. (2), plotted against the square of the electric field.

sion and the magnitude of the birefringence immediately prior to interrupting the field, there being a significant remnant of birefringence that persists to very long times at high fields. The randomization time is entirely a product of Brownian dissipation and is orders of magnitude larger than the field driven orientation time. The rate of randomization is not exponential, as seen clearly in Figs. 3, 5, 7, and 8, and requires a complex description.

IV. DISCUSSION

A. Theory

To discuss all of these results we first consider the classical description as given by Benoit[13] and Doi and Edwards.[14] In this description of the magnitude, rise and fall of the birefringence upon application of an electric field and its subsequent removal are given, respectively, by

$$\Delta n_R(t) = K_0 n E^2 \left(1 - \frac{3R}{2(R+1)} \exp(-2D_R t) + \frac{R-2}{2(R+1)} \exp(-6D_R t) \right) \tag{3a}$$

and

$$\Delta n_F(t) = K_0 n E^2 \exp(-6D_R t), \tag{3b}$$

where D_R is the rotational diffusion coefficient for rotation about an axis perpendicular to the long axis for an elongated particle with axial symmetry and large aspect ratio.

The rotational diffusion coefficient is given by

$$D_R = \frac{k_B T}{\zeta_R} = \frac{3k_B T \left[\ln\left(\frac{L}{b}\right) - \kappa \right]}{\pi \eta_S L^3}. \tag{4}$$

Where ζ_R is the rotational friction coefficient and η_S is the viscosity of the suspending medium and L is the nanotube length[15,16]

$$\zeta_R = \frac{\pi \eta_S L^3}{3\left[\ln\left(\frac{L}{b}\right) - \kappa \right]}, \tag{5}$$

K_0 is the Kerr coefficient, and $K_0 n E^2 \equiv \Delta n_\infty$ as used earlier in the results section. n is the average refractive index or refractive index of the solvent. R is a measure of the ratio of permanent to induced contribution to the dipole moment

$$R = \frac{\mu^2}{\Delta\alpha k_B T}, \tag{6}$$

where μ is the permanent dipole and $\Delta\alpha = \alpha_\parallel - \alpha_\perp$ is the difference between the axial and radial polarizability. κ is a correction factor of order unity (≈ 0.8 for rigid rods).

For a solution or suspension as in this work we define a specific Kerr coefficient K_{SP} in order to take into account the volume fraction C_V of the nanotubes

$$K_{SP} = \frac{K_0}{C_V}. \tag{7}$$

Following O'Konski,[17] K_{SP} is given[18,19] in terms of molecular properties of a solute by

$$\Delta n = \frac{2\pi C_V}{n} \Delta g \Phi, \tag{8}$$

where $n = 1.44$ is the refractive index of the suspending medium DCE and $\Delta g = (g_\parallel - g_\perp)$ is the optical polarizability anisotropy per unit volume of the nanotubes. Φ is an alignment function or order parameter that is determined by electric field and permanent and induced dipole moments

$$\Phi = \frac{3\int_{-1}^{1} u^2 \exp(\beta u + \gamma u^2) du}{2\int_{-1}^{1} \exp(\beta u + \gamma u^2) du}, \tag{9}$$

where $u = \cos\theta$, $\beta = \mu E / k_B T$, and $\gamma = (\Delta\alpha / 2k_B T) E^2$. θ is the angle made by the tube with the electric field vector.

At low fields the exponentials in Eq. (9) may be expanded in a power series in E to give

$$\Phi = \frac{\beta^2 + 2\gamma}{15} = \frac{1}{15}\left(\frac{\mu^2}{k_B^2 T^2} + \frac{\Delta\alpha}{k_B T} \right) E^2, \quad E \ll E_{\mathrm{SAT}} \tag{10}$$

and

$$K_{SP} = \frac{2\pi}{15n} \Delta g \left(\frac{\mu^2}{k_B^2 T^2} + \frac{\Delta\alpha}{k_B T} \right), \quad E \ll E_{\mathrm{SAT}}. \tag{11}$$

For carbon nanotubes for which the permanent dipole $\mu = 0$ Eq. (11) may be simplified.

$$K_{SP} = \frac{2\pi}{15n} \Delta g \frac{\Delta\alpha}{k_B T}. \tag{11a}$$

At high enough fields $\Phi \to 1$ and

$$\frac{1}{C_V} \Delta n_\infty (E \to \infty) = \frac{2\pi}{n} \Delta g, \quad E \to \infty. \tag{12}$$

We note that when there is no permanent dipole moment then $R \equiv 0$ and Eqs. (3a) and (3b) give a rise and fall that are symmetric with both Eqs. (3a) and (3b) being replaced by

$$\Delta n_{R/F} = K_0 n E^2 [1 - \exp(-6D_R t)] \tag{13}$$

with a characteristic exponential time constant of $\tau = (6D_R)^{-1}$ describing both the rise and fall.

Such a description has been widely used in explaining birefringence in systems varying from the tobacco mosaic virus with symmetric rise and fall times to studies of CdSe nanorods[20] where the fall time is considerably faster than the rise time. It has been noted in Ref. 20 that Eqs. (3a) and (3b) imply that the fall time can only be faster than the rise time in the case where there is a permanent dipole moment along the long axis of the particle, i.e., that the CdSe nanorods have such a permanent dipole. There is no permanent dipole for carbon SWNTs and $R \equiv 0$. However the rise and fall times are very clearly asymmetric in contrast to the predictions of the theory, i.e., in this work the third possibility is observed that the fall time is the longer of the two. This possibility in the absence of a permanent dipole is not covered by the preceding theory. In fact the fall time is orders of magnitude longer and is not describable by a single exponential. This is due to the fact that the fall time described by Benoit through Eq. (3b) is applicable to a dilute, monodisperse system where there is one rotation diffusion coefficient describing all of the particles. The system under study here is far from monodisperse, requiring a more complicated description, and is indeed even more complex, containing both metallic and semiconducting nanotubes of varying band gap together with their very differently behaved optical factors. Because of this complexity in the sample we are unable to say much more about the fall time, determined as it is by the rotational diffusion of rods with a wide range of lengths. We will from now on concentrate on the rise time.

The rise time is observed to have the following properties.

(1) It is independent of concentration at all fields used here as seen in Figs. 3 and 5 indicating that we are observing single particle properties.

(2) The rise time is much faster than the fall time in spite of the absence of permanent dipole moments on carbon SWNTs.

(3) It displays a monoexponential growth in contradiction to the polydisperse nature of the sample and the various D_R that are present as a consequence.

(4) It is inversely proportional to the square of the applied electric field at low fields. To our knowledge this observation of a field dependent on the rise time is a unique behavior in studies of the Kerr effect to SWNTs, alignment times being governed entirely by Brownian forces and the rotational diffusion of the particle as described by Eq. (3a).

We present a simple explanation of all of these observations. We begin by noting that the polarizability per unit length of the semiconducting and metallic rods are given by[21,22]

$$\alpha^S = \left[\frac{8\pi\hbar^2 e^2}{mA}\right]\left(\frac{b}{\tilde{E}_G^2}\right), \tag{14}$$

where $\tilde{E}_G \approx 5.4 E_G$ (E_G being the semiconductor band gap) and

$$\alpha^M = \frac{L^2}{24\left(\ln\frac{L}{b} - 1\right)}\left(1 + \frac{4/3 - \ln 2}{\ln\left(\frac{L}{b}\right) - 1}\right). \tag{15}$$

For typical tube dimensions used in this work ($L/b \approx 10^3$) the metallic tube polarizability is three orders of magnitude greater than that of semiconductors. Thus, while a typical nanotube sample is made up of semiconductor:metal in the ratio of 2:1, because of the much larger polarizability of the metals we make the plausible assumption that the effects that we observe are governed entirely by the metallic tubes. We further assume that unlike the fall time, the rise time is not controlled by the Brownian motion given the large size of the aligning field and/or polarizability and the mass and/or moment of inertia of the particles involved. In neglecting Brownian forces we may equate the torque to the rotational friction force to find the angular velocity, ω.

$$\vec{T} = -(\alpha^M \vec{L} \cdot \vec{E}\hat{L}) \times \vec{E} = \zeta_R \vec{\omega}, \tag{16}$$

where the unit vector on the direction of the long axis of the nanotube, $\hat{L}$, is included to bring out the vectorial nature of the equation.

Using Eqs. (5) and (15) and recalling the angle θ, between the long axis and the applied electric field we may rewrite Eq. (16)

$$\frac{-E^2 L^3}{24\left(\ln\frac{L}{b} - 1\right)}\left(1 + \frac{4/3 - \ln 2}{\ln\left(\frac{L}{b}\right) - 1}\right)\cos\theta \sin\theta = T = \frac{\pi \eta_S L^3}{3\left[\ln\left(\frac{L}{b}\right) - \kappa\right]}\omega. \tag{17}$$

Using the fact that the correction factor $\kappa \approx 0.8$ for rigid rods, Eq. (17) is simplified

$$\frac{-E^2}{16}\left(1 + \frac{0.636}{\ln\left(\frac{L}{b}\right) - 1}\right)\sin 2\theta = \pi \eta_S \omega. \tag{18}$$

Given a value for $\ln(L/b) = 6.54$ for tubes of 1 μm length and the very slow variation of $\ln(L/b)$ with length we can write

$$\frac{d\theta}{dt} = \frac{-E^2}{16\pi\eta_S}\sin 2\theta. \tag{19}$$

We note that the L^3 dependence for the polarizability of metal rods on the LHS of Eq. (17) and the L^3 that appears in the rotational friction coefficient on the RHS have canceled each other and the value of ω does not depend on L thus removing the paradox noted earlier that our samples are polydisperse and yet we have a monoexponential growth.

Furthermore, the angular velocity is proportional to the square of the electric field according to Eq. (19). While it is not a straightforward matter to solve Eq. (19) and obtain a growth rate from the angular velocity we can find the time taken to go from θ_1 to θ_2 by integrating Eq. (19):

$$\int_{\theta_1}^{\theta_2} \frac{d\theta}{\sin 2\theta} = \frac{1}{2} \ln(\tan\theta)\Big|_{\theta_1}^{\theta_2} = \frac{-E^2}{16\pi\eta_S}\int_{t_1}^{t_2} dt = \frac{-E^2}{16\pi\eta_S}(t_2 - t_1) \tag{20}$$

and we find that the time constant is proportional to E^{-2}

$$\exp\left(\frac{-E^2}{16\pi\eta_S}(t_2 - t_1)\right) = \frac{\tan\theta_2}{\tan\theta_1} \tag{21}$$

as found experimentally at low fields where the Kerr effect is operating. At higher fields where alignment begins to saturate the Kerr effect we can no longer use Eq. (19) to find a field dependence for the rise time.

The induced birefringence tends to saturation at the higher fields used in these experiments. This is indicative of the fact that the tubes are easily aligned and are expected to occur at fields large enough that the field dipole energy overcomes the Brownian forces experienced by the tubes. In the case of SWNTs, the tubes are long and highly polarizable and also have a large moment of inertia; this saturation is found to occur at moderate fields. To observe a birefringence varying with the square of the magnitude of the field and thus corresponding to the low field Kerr effect we need to go to very low electric fields, Fig. 11. From the slope of the data in Fig. 11 at low fields we can obtain $K_0 = 1.4 \times 10^{-18}$ m^2 V^{-2} as defined through Eqs. (3a) and (3b) and find for metallic SWNTs that $K_{SP} = 2.0 \times 10^{-12}$ m^2 V^{-2} ($=1.8 \times 10^{-3}$ esu). We note that the values of the Kerr coefficient will depend on the length of nanotube and the value given here is the average value for the collection of lengths present in these samples. It should also be noted that we have used a value for $\boldsymbol{C_V}$ that takes account of both metallic and semiconducting nanotubes whereas we are assuming that the metallic tubes are the dominant species in these measurements. The value of K_{SP} found here is of the same order of magnitude as that found for Tobacco Mosaic Virus, TMV,[23] by O'Konski *et al.* who find 1.36×10^{-3} esu for TMV and about two orders of magnitude greater than that found for the polypeptide alpha helix, poly-γ-benzyl-L-glutamate where $K_{SP} = 1.3 \times 10^{-5}$ esu.[24] The size of the Kerr coefficient is clearly the reason why we are able to ignore Brownian forces in the alignment regime of these experiments Because of this large value for K_{SP} we have a very clear saturation behavior of Δn_∞ with E^2 seen in Fig. 11, we may use Eq. (12) and the value of Δn_∞ at infinite field found from extrapolation in Fig. 12, to analyze further these results. By noting that $\Delta\alpha$ only appears through its role in the alignment process and that with full alignment of the particles can play no further part we may use Eq. (12) to find the value of $\Delta \boldsymbol{g}$ the optical anisotropy using the extrapolated value of Δn_∞ at an infinite field from Fig. 12. $\Delta n_\infty (E \to \infty) = 3.8 \times 10^{-8}$ at infinite field and we find $\Delta g = (n/C_V)(1/2\pi)\Delta n_\infty(E \to \infty) = 1.24 \times 10^{-2}$.

V. CONCLUSIONS

Nanotubes are expected to act as true rigid rods and thus to offer the possibility of testing theories of the Kerr effect where the rigid rod was taken as the paradigm on which to model behavior of complex systems. Previously such systems have included the tobacco mosaic virus as the ideal rigid rod and others including the polypeptide alpha helix and DNA which were both reasonable approximations to rigid rods. We have studied the Kerr effect on SWNTs and found a number of interesting behaviors and properties.

1. That metallic tubes dominate the behavior and that the Kerr effect normalized to the volume fraction of the sample is one of the largest known Kerr coefficients, being of the same order of magnitude as that of TMV.

2. A polydisperse sample behaves with the simplicity of a monodisperse sample.

We have offered an explanation for this observation that requires that the particles of interest are the metallic nanotubes on which dipoles are induced. It also requires that during the alignment of the tubes we may neglect any action due to Brownian forces.

3. That the rise time varies as the reciprocal square of the aligning field at low fields.

As a consequence of the previous explanation this second observation is explained as the angular velocity of a metallic tube is shown to be proportional to the square of the field.

The fall time is complex and displays the following behaviors.

1. It is much longer than the rise time, an observation generally taken to indicate that induced dipoles are involved.

2. Birefringence after application of high fields and achievement of large birefringence has a remnant for a long time after an initial fall indicating a persistence of alignment. This is possibly due to some co-operative phenomena such as filament formation among aligned SWNTs.

3. After application of low fields the birefringence falls away more rapidly although the situation is a little more complicated at high concentrations.

To make progress in the study of the fall time, allowing determination of the rotational diffusion coefficient, will require a finer control over the tube length, and we are currently working on experiments where the polydispersity of the current sample is significantly reduced. It is also necessary to improve techniques in order to study less concentrated samples where the birefringence is more clearly linear in concentration.

We initially carried out these experiments to try and understand some observations made in studies on transient photocurrents[5,6] suggesting that alignment in the electric field was increasing the carrier Schubweg or range which is an important factor in determining the magnitude of the photocurrent. In this case the range to be used is the range projected onto the field direction. As isolated tubes orient with the field, this projection increases. However those experiments were carried out with the field on for a few tens of microseconds before the laser pulse that excited the photocurrent and the tubes had little chance to significantly orientate. However, the observation of the remnant birefringence does have implications for the transient photocurrent mea-

surements as they were frequently made by averaging over a large number of laser/voltage pulses with a repetition rate of typically 1 Hz. The implications of this need to be explored further in the future.

ACKNOWLEDGMENT

One of us, K.J.D., would like to thank Dr. Bob Jones for invaluable discussions.

*Corresponding author. Email address: k.j.donovan@qmul.ac.uk

[1] S. Iijima, Nature (London) **354**, 56 (1991).
[2] L. X. Benedict, S. G. Louie, and M. L. Cohen, Phys. Rev. B **52**, 8541 (1995).
[3] R. Krupke, F. Hennrich, H. v. Löhneysen, and M. M. Kappes, Science **30**, 344 (2003).
[4] T. Lutz and K. J. Donovan, Carbon (to be published).
[5] J. C. Bunning, K. J. Donovan, and K. Scott, J. Appl. Phys. **96**, 3939 (2004).
[6] J. C. Bunning, K. J. Donovan, K. Scott, and M. Somerton, Phys. Rev. B **71**, 085412 (2005).
[7] L. A. Nagahara, I. Amlani, J. Lewenstein, and R. K. Tsui, Appl. Phys. Lett. **80**, 3826 (2002).
[8] K. Yamamoto, S. Akita, and Y. Nakayama, J. Phys. D **31**, L346 (1998).
[9] L. Jingqi, Z. Qing, N. Peng, and Z. Qi, Appl. Phys. Lett. **86**, 153116 (2005).
[10] P. Avouris, Chem. Phys. **281**, 429 (2002).
[11] K. Bubke, H. Gnewuch, M. Hempstead, J. Hammer, and M. L. H. Green, Appl. Phys. Lett. **71**, 1906 (1997).
[12] L. C. Venema, V. Meunier, Ph. Lambin, and C. Dekker, Phys. Rev. B **61**, 2991 (2000).
[13] H. Benoit, Ann. Phys. (Paris) **6**, 561 (1951).
[14] M. Doi and S. F. Edwards, *The Theory of Polymer Dynamics*, International Series of Monographs on Physics Vol. 73 (Clarendon, Oxford, 1986).
[15] C. W. Oseen, *Hydrodynamik* (Akademische Verlagsgesselschaft m.b.H., Leipzig, 1927), p. 35.
[16] S. Broersma, J. Chem. Phys. **32**, 1626 (1960).
[17] C. T. O'Konski, *Molecular Electro-Optics*, edited by S. Krause, NATO Advanced Studies Institute, Series B: Physics (Plenum, New York, 1981), Vol. 64, p. 119.
[18] D. N. Holcomb and T. Tinoco, Biopolymers **3**, 121 (1965).
[19] F. Fredericq and C. Houssier, *Electric Dichroism and Electric Birefringence* (Clarendon, Oxford, 1973).
[20] L. Li and A. P. Alivisatos, Phys. Rev. Lett. **90**, 097402 (2003).
[21] L. D. Landau, E. M. Lifshitz, and L. P. Pitaevskii, *Electrodynamics of Continuous Media* (Pergamon, Oxford, 1981).
[22] E. Joselevich and C. M. Lieber, Nano Lett. **2**, 1137 (2002).
[23] C. T. O'Konski, K. Yoshioka, and W. H. Orttung, J. Chem. Phys. **63**, 1558 (1959).
[24] S. Krause and C. T. O'Konski, Biopolymers **1**, 503 (1963).